Comprehensive Modeling of a Liquid Rocket Combustion Chamber

Pak-Yan Liang,* Steven Fisher,† and Y. Mason Chang‡
Rockwell International, Canoga Park, California

An analytical model for the simulation of three-phase transient combustion flows is presented. The three phases are: 1) multispecies gas, 2) incompressible liquid, and 3) particulate droplet. The gas and liquid phases are continuum described in a Eulerian fashion. A two-phase solution capability for these continuous media is obtained through a marriage of the implicit continuous Eulerian technique and the fractional volume of fluid free-surface description method. On the other hand, the particulate phase is described in a discrete Lagrangian fashion. All three phases are hence treated rigorously. Physical models are used to describe all interphase coupling terms as well as the chemistry among gaseous components. Sample calculations using the model are given. The results show promising application to comprehensive modeling of liquid-fueled engine systems.

Nomenclature

B_A = empirical constant for atomization drop size
c = speed of sound
C_A = empirical constant for atomization rate
C_v = specific heat at constant volume
D = diffusivity
D_j = liquid jet diameter
$\mathfrak{D}_k$ = droplet drag per unit relative velocity
F = fractional volume of gas, Eq. (15)
G = body force
h = specific enthalpy
H = droplet specific enthalpy
I = specific internal energy; identity matrix
K = thermal conductivity
K_D = turbulence model empirical constant, $=O(0.1)$
Le = Lewis number
m = droplet mass
M = mass of gas in cell
$\mathfrak{M}$ = molecular weight
Nu = Nusselt number
P = pressure
Pr = Prandtl number
r = droplet radius; or radial coordinate $=x$ if cylindrical, $=1$ if two-dimensional
R = universal gas constant
Re = Reynolds number
S = pressure difference during iteration, Eq. (24)
$\mathcal{S}$ = droplet momentum coupling term
Sc = Schmidt number
S_w = droplet angular momentum coupling term
t = time
T = temperature
u,v,w = gas velocity components
U,V,W = droplet velocity components
V = volume (without subscript)
y = axial coordinate; or species mass
ϵ = turbulent kinetic energy level for droplet dispersion
Λ = cell scale length for turbulence model
μ,λ = viscosity
ρ = density
σ = viscous stress tensor; surface tension
τ = turbulence time scale for droplet dispersion
∇ = differentiation operation, $i\frac{\partial}{\partial x}+j\frac{\partial}{\partial y}$

Subscripts

$\approx$ = tensor quantity
k = species number; droplet number
ℓ = liquid
r = relative
0 = gaseous mixture exclusive of oxygen
1 = species 1 = oxygen

Superscripts

$( )^*$ = properties at droplet surface
i = iteration index

Introduction

COMBUSTION chambers involving liquid propellants represent one of the most complicated engineering flow systems in operation. The complexity stems from the existence of multiple zones and dominant processes with very different time and length scales within the same physical domain (Fig. 1). The zones are in close proximity to each other and the processes are strongly coupled. In the injection zone, for instance, the major physical characteristics include those of two-phase gas/liquid flow, recirculation, high shear stresses, and steep pressure gradients. The dominant processes are liquid jet breakup and atomization, droplet interactions, and fluid-wall interactions. A short distance away from the injector, however, the dominant characteristics of the flow become those of steep concentration gradients around droplets, turbulent mixing and diffusion, and two-phase gas/droplet flow. The critical processes become those of droplet transport, evaporation, and droplet heatup. Further downstream, the fuel/oxidizer mixture begins to combust. The flow is now characterized by large heat fluxes, a large number of species, and temperature extremes that necessitate the consideration of real gas properties. The key processes are kinetic and equilibrium chemical reactions and species diffusion. Finally, in the post-combustion or expansion zone, the fluid properties range from a "frozen" composition to near "dynamic equilibrium." There is a high-velocity gradient near the walls and at the nozzle. The dominant processes of interest are transonic/supersonic flows and boundary-layer effects.

Presented as Paper 85-0232 at the AIAA 23rd Aerospace Sciences Meeting, Reno, NV, Jan. 14-17, 1985; received Jan. 30, 1985; revision received Aug. 5, 1985.

*Member Technical Staff, Flow Systems Analysis, Rocketdyne Division. Member AIAA.
†Project Engineer, Turbo-Drive Technology, Rocketdyne Division.
‡Project Engineer, Flow Systems Analysis, Rocketdyne Division.

Thus far, existing models[1-5] for performance analysis of rocket combustion have tended to decouple these critical processes. While they are useful for economical prediction of performance data, the methodologies used are those available prior to the recent advances in large-scale, finite difference modeling. A summary of some of these programs is listed in Table 1. More recent attempts in combustion modeling (e.g., Refs. 6 and 7) have utilized finite difference schemes for solutions of the fluid-dynamical equations and coupled them with relatively sophisticated combustion models. However, droplets are often treated as an additional species of the continuous medium and characteristics of the spray are supplied to the model as inputs. These models produced satisfactory results for air-breathing turbine and internal combustion (IC) engine combustors.

The spray characteristics inside a high-performance liquid rocket engine, such as the Space Shuttle main engine (SSME), differ from those of a typical spray in that the atomization process is not complete at the injector exit. The internal diameter of a typical coaxial rocket injector is of the order of 0.25 cm, as compared with the submillimeter size of a more conventional injector. As a result, a stream of liquid (in this case liquid oxygen) would enter the combustion chamber before it is atomized by the shearing action of the surrounding high-speed concentric gas stream (hydrogen). The liquid takes up a non-negligible volume locally that must be accounted for in the fluid-dynamic calculations. The atomized spray also consists of droplets that take up substantial volume. In other words, a thin spray assumption is no longer applicable. Initial droplet spray characteristics are not known, droplets are created over an extended area, and a point droplet source simplification would be unsatisfactory.

The model described here attempts to overcome these difficulties and enhance the realism of the resulting description.

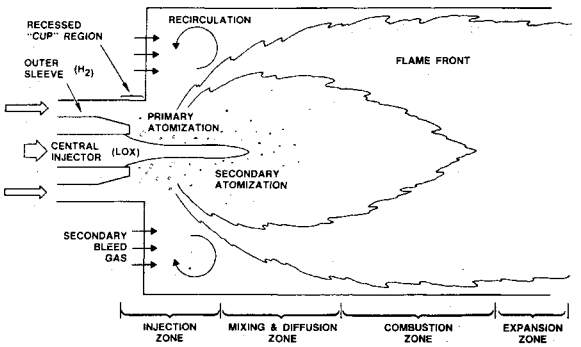

Fig. 1 Various zones within a coaxial injector/combustor.

A true three-phase (liquid, gas, particles) capability is developed, droplets of finite volume are tracked in a Lagrangian fashion to eliminate numerical diffusion, and the atomization process is modeled rather than prescribed as an empirical input. The model is transient and currently restricted to axisymmetric configurations with swirl, although extension to a full three-dimensional model is planned. Parts of the development effort have been outlined in previous reports.[8,9]

Governing Equations

Liquid and Gas Phases

The gaseous phase consists of a multiple-species compressible mixture, while the liquid phase is assumed to be incompressible with a constant density and temperature. The continuity equations are

$$\frac{\partial \rho_k}{\partial t}+\frac{1}{r}\nabla\cdot(r\rho_k u)=\underbrace{\frac{1}{r}\nabla\cdot[r\rho D\nabla(\rho_k/\rho)]}_{\text{diffusion}}+\underbrace{\dot{\rho}_k^C}_{\text{chemistry}}+\underbrace{\dot{\rho}_S\delta_{k1}}_{\text{evaporation}} \tag{1}$$

for the gas component k, and

$$\frac{1}{r}\nabla\cdot(r\boldsymbol{u})=0 \tag{2}$$

for the liquid. The gas mixture obeys the summation rules of

$$\rho=\sum_k \rho_k \tag{3}$$

$$I=\sum_k (\rho_k/\rho)I_k \tag{4}$$

$$C_v=\sum_k (\rho_k/\rho)C_{vk} \tag{5}$$

$$h=\sum_k h_k=\sum_k [I_k+RT/\mathfrak{M}_k] \tag{6}$$

$$P=RT\sum_k (\rho_k/\mathfrak{M}_k) \tag{7}$$

The momentum equations for both the gas and liquid phases are given by

$$\frac{\partial(\bar{\rho}\boldsymbol{u})}{\partial t}+\frac{1}{r}\nabla\cdot(r\bar{\rho}\boldsymbol{u}\boldsymbol{u})=-\nabla P+\frac{1}{r}\nabla\cdot(r\underset{\approx}{\sigma})-\frac{(\sigma_0-\bar{\rho}w^2)}{r}\nabla r+\mathcal{S}+\bar{\rho}\boldsymbol{G} \tag{8}$$

Table 1 Earlier-generation rocket combustion codes

Code	Primary functions	Major limitations
CICM[1]	Steady-state rocket combustion of H_2/LOX for coaxial injection	Streamtube fluid dynamics Atomization correlations from J-2 engine
TRANS78[2]	Multipurpose chemistry code for rocket performance, detonation, constant P or constant V combustion, etc.	One-dimensional equilibrium isentropic. No spatial resolution or flow dynamics.
SDER[3]	Steady-state one-dimensional fluid dynamics with three-dimensional droplet dynamics for impinging-type elements. Liquid/gas, subcritical and supercritical vaporization of droplets	Droplet correlations developed from cold flow. Streamtube fluid dynamics
TPP[4]	Time-dependent program for small pulsed-type engines with hypergolic propellants. Three-dimensional droplet dynamics	One-dimensional fluid dynamics. Impinging liquid-liquid elements only. Subcritical droplets
GKAP[5]	Steady-state chemically reacting gas mixtures of up to 150 species and 70 nonequilibrium reactions	One-dimensional flow. Adiabatic combustion chamber. No droplets

where $\underset{\approx}{\sigma}$ and σ_0 are the two-dimensional tensor and cylindrical viscous stresses, respectively. The density $\bar{\rho}$ used in the evaluation of the above equation is a cell volume averaged density defined in the next subsection. The viscous stresses are given by

$$\underset{\approx}{\sigma} = \mu(\underset{\approx}{\text{def}}\boldsymbol{u}) + (\lambda/r)\nabla\cdot(r\boldsymbol{u})\underset{\approx}{I} \tag{9}$$

$$\sigma_0 = (2\mu/r)\boldsymbol{u}\cdot\nabla r + (\lambda/r)\nabla\cdot(r\boldsymbol{u}) \tag{10}$$

where $\underset{\approx}{\text{def}}\,\boldsymbol{u}$ = velocity deformation $= \nabla\boldsymbol{u} + (\nabla\boldsymbol{u})^T$.

For axisymmetric flow with swirl, the two-dimensional Navier-Stokes equations are supplemented with the angular momentum equation

$$\frac{\partial(r\bar{\rho}w)}{\partial t} + \frac{1}{r}\nabla\cdot(r^2\rho w\boldsymbol{u}) = \frac{1}{r}\nabla\cdot(r\tau) + S_w \tag{11a}$$

where

$$\tau = \mu r^2\nabla(w/r) \tag{11b}$$

Finally, the equation for internal energy is given by

$$\frac{\partial(\rho I)}{\partial t} + \frac{1}{r}\nabla(r\rho I\boldsymbol{u}) = -\frac{P}{r}\nabla(r\boldsymbol{u}) + \underset{\approx}{\sigma}:\nabla\boldsymbol{u} + \tau\cdot\nabla(w/r)$$

$$+\frac{\sigma_0}{r}\boldsymbol{u}\nabla r - \frac{1}{r}\nabla\cdot(r\boldsymbol{J}) + \dot{Q}_{\substack{\text{chem-}\\\text{istry}}} + \dot{Q}_{\text{spray}} \tag{12}$$

where the heat flux consists of both conduction and diffusion terms

$$\boldsymbol{J} = K\nabla T - \rho D\sum_k h_k\nabla(\rho_k/\rho) \tag{13}$$

Note that ρ, not $\bar{\rho}$, is used in the energy equation as the liquid is assumed to have constant temperature and does not participate in the energy exchange.

Volume of Fluid Methodology

The presence of gas and liquid phases separated by a deforming free-surface boundary presents an additional challenge and warrants the adoption of special schemes to describe this phenomenon. In an Eulerian finite difference grid, the free surface will inevitably cut through the sides of a computational cell partitioning it into subcell regions with different properties. Thus, a workable scheme for free-surface flows must be able to identify and track the location of this free surface and preserve its identity as it moves through the grid, i.e., numerical diffusion of the sharp boundary must be minimized. One scheme that has been applied successfully to this task is the fractional volume of fluid (VOF) method.[10] This method utilizes an additional variable, F, to designate the fraction of the cell volume occupied by one of the two nonmixing fluids. The distribution of the value of F over a cell and its neighbors will define the location and orientation of the free surface. In the current scheme, a general active (nonsolid) cell can have its volume taken up by droplets, gaseous mixture, and incompressible liquid (Fig. 2). In other words,

$$V_{\text{cell}} = V_{\text{gas}} + V_{\text{liq}} + V_{\text{droplets}} \tag{14}$$

and the variable F is defined as

$$F = V_{\text{gas}}/(V_{\text{gas}} + V_{\text{liq}}) \tag{15}$$

It may be noted that defined this way, F is in fact the volume average of an intrinsic fluid property $\hat{F}$ that takes on the value of either 0 or 1 and moves with the fluid, thus satisfying the conservation equation of

$$\frac{\partial\hat{F}}{\partial t} + \frac{1}{r}\nabla\cdot(r\boldsymbol{u}\hat{F}) + \dot{F}_S = 0, \quad \hat{F} \equiv \lim_{V\to 0} F \tag{16}$$

where $\dot{F}_S$ is a source term to account for the depletion of liquid from the atomization process. When averaged over a cell volume, F would, of course, take on any value between 0 and 1. With F available, the averaged cell density required in the solution of the momentum equation (7) is calculated as

$$\bar{\rho} = F\rho + (1-F)\rho_\ell \tag{17}$$

It should be mentioned that the VOF technique as used in Ref. 10 concerns itself only with the computation of the liquid phase, which is assumed to be surrounded by either a vacuum or an inert gas of constant pressure. In the present model, we are dealing with a compressible gas of changing pressure. Inside any computational cell where both gas and liquid are present, the two are coupled together. In determining the final velocity, a suitable solution method must be capable of distinguishing between the part of the cell volume that exhibits compressible behavior and the part that does not. Furthermore, in the context of finite difference approximations, the smearing of the F function must be avoided by use of a donor-acceptor fluxing method that preserves the discontinuous nature of F. Fortunately, both of these requirements lend themselves to ready accommodation by the three-step implicit continuous-fluid Eulerian (ICE) technique used in a number of general-purpose flow programs for all flow speeds.[11,12] The resulting marriage of ICE and VOF is the approach adopted in the current model.

Discrete Particle Phase

Since the particles are discrete and tracked in a Lagrangian fashion, they are governed by straightforward ordinary differential equations. Once created by atomization, mass conservation is simply

$$\frac{dm_k}{dt} = \dot{m}_{\text{evap}} \tag{18}$$

where $\dot{m}_{\text{evap}}$ is described by an empirical physical model described later.

Momentum conservation is

$$\frac{d\boldsymbol{U}_k}{dt} = \frac{\mathfrak{D}_k}{m_k}(\boldsymbol{u} - \boldsymbol{U}_k) + \frac{W_k^2}{r}\nabla r = \boldsymbol{G}_k \tag{19}$$

where $\boldsymbol{G}_k$ is the body force or "bouyancy" term. When a swirl component is present, it is given by

$$\frac{dW_k}{dt} = \frac{\mathfrak{D}_k}{m_k}(w - W_k) - \frac{U_k W_k}{r_k} \tag{20}$$

Lastly, the droplet energy conservation is described by

$$m_k\frac{dH_k}{dt} = L(T_k)\frac{dm_k}{dt} + q_k \tag{21}$$

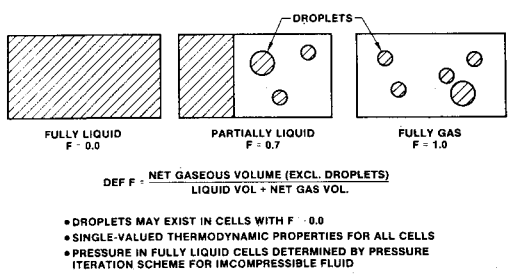

Fig. 2 Different types of active cells in two-phase advanced rocket injector combustor code.

where $L(T_k)$ is the latent heat of vaporization and q_k the rate of heat transfer to the droplet from the surrounding gas, also based on physical modeling.

To conserve computer storage the "Monte Carlo" droplet group representation[13] is used. These equations, together with the fluid-phase equations and the semiempirical physical models, form a complete description of the three-phase combusting flow system.

Summary of Solution Procedure

The current model is an extension of the CONCHAS-SPRAY[14] combustion code developed for IC engines. The basic solution algorithm is a modified three-step ICE technique. The first step—the explicit updating of the velocity components from all of the contributing terms of the momentum equations except the convective terms—is essentially the same as the original ICE procedure. The overall algorithm is made implicit in the second step through a successive overrelaxation (SOR) iteration procedure. Still Lagrangian in nature as the first step, this process couples the momentum equations with the continuity equation as the new control volumes are used to determine the change in density and, through the state equation, the cell pressure. Rewriting Eq. (7),

$$\hat{P}=RT^{i+1}\sum_k(\rho_k)^{i+1}\Big/\mathfrak{M}_k, \quad i=\text{iteration index} \tag{22}$$

and the updated pressure is

$$P^{i+1}=P^i+\Delta P=P^i-S\cdot\left(\frac{\partial S}{\partial P}\right)^{-1}\cdot\omega \tag{23}$$

where

$$S\equiv P^i-\hat{P} \tag{24}$$

$$\rho_k^{i+1}=\rho^0(V^0/V^{i+1}) \tag{25}$$

$$T^{i+1}=T^0+(I^{i+1}-I^0)/C_v^0 \tag{26}$$

$$I^{i+1}=I^0-P^i(V^{i+1}-V^0)/M \tag{27}$$

and

$$\omega\sim O(1)=\text{a relaxation coefficient}$$

The term $(\partial S/\partial P)$ is determined for each cell before the iteration process by introduction of a small arbitrary ΔP into the cell. The new pressure will then be used to update the cell vertex positions and, hence, the cell volumes.

Now, the state equation [Eq. (22)] is applicable only to the gaseous portion of the flow. It is assumed that cells that are at least partially gaseous have their pressure dictated by the gas pressure that is determined by the above procedure and then assigned uniformly to the entire cell. It should be noted that the volume change being considered in the pressure iteration [Eq. (25)] is that of the net gaseous volume, as the liquid- or droplet-occupied portions of the cell are assumed to be incompressible. It can happen, however, that as the flow develops a cell will become largely occupied by liquid and droplets, leaving only a tiny gaseous "pocket" in the cell and, hence, making the cell pressure extremely sensitive to minute changes in velocities or cell volume. Under such circumstances (the criterion currently set at $F<0.1$), the "incompressible" iteration described next is used, and the fluid inside the cell is treated as basically incompressible.

For incompressible flows, the ideal gas equation does not apply and, indeed, only relative pressure levels, not absolute pressure, are defined. Instead of switching to an extremely rigid liquid state equation, we follow a recommendation given by Ref. 11 along the lines of a "pseudoincompressible" treatment and determine the new pressure in a certain iteration as

$$S=\rho_\ell c^2(V^{i+1}-V^i)/V^i \tag{28}$$

where the coefficients $\rho_\ell c^2$ can, in principle, be any suitably large number, convert the small volume changes into appropriately large pressure changes. The choice of $\rho_\ell c^2$ reflects a temporary acoustic compressibility, as can be deduced by inclusion of a limited compressibility term described below. The volume being considered now is the entire cell volume. From the above equation, it can be seen that convergence will be achieved only when changes in the cell volume cease to exist. Furthermore, as the whole solution scheme is elliptic in nature and each cell is coupled to all of its neighboring cells, the pressure inside a liquid cell will also take on an absolute value through coupling with neighboring cells that are partially gaseous or at a boundary. The above procedure works well where no steep pressure gradients are involved. If strong pressure gradients do exist (e.g., when a shock passes over the liquid), or when it is necessary to account for acoustic waves traveling inside the liquid phase, it is found desirable to include a "limited compressibility" term in the liquid-phase continuity equation. Namely, Eq. (2) is modified to

$$\frac{1}{\rho_\ell c^2}\frac{\partial P}{\partial t}+\frac{1}{r}\nabla(ru)=0 \tag{29}$$

and the iteration step in Eq. (28) is also adjusted accordingly:

$$S=\rho_\ell c^2(V^{i+1}-V^i)/V^i+(P^i-P^0) \tag{30}$$

The inclusion of limited compressibility makes the liquid iteration process more stable and allows much faster convergence benefits, refer to Ref. 15.

Finally, in the third step of the ICE algorithm, Lagrangian values are converted back to Eulerian through evaluation of the convective fluxes. The only special treatment required is when partially liquid cells are involved. In such cases, to preserve the sharpness of the interface and coherence of the liquid medium, careful consideration must be given to decide whether the acceptor or the donor cell F value should be used in determining the fractional makeup of the volume fluxed across the boundary. As discussed in Ref. 10, the acceptor cell F is used when the surface is advected mostly normal to itself, while the donor cell F is used when the surface is advected along itself. In our current model, since we are dealing primarily with an axial liquid jet, it is assumed that convection in the radial direction is mostly normal to the liquid surface and convection in the axial direction is mostly tangential to the liquid surface. However, if the acceptor cell is devoid of liquid and the donor cell is less than 50% filled with liquid, then the acceptor cell F is always used. The last provision prevents the formation of an elongated jet of infinitesimally small radius and results in a relatively well-shaped conical jet tip. Figure 3 is a schematic depicting the choice of F. In addition to the preceding logic, two limiting conditions must be set:

$$\Delta V_{\text{liq}}=\min\{(1-F_{AD})\Delta V+\mathfrak{F}, V_{D,\text{liq}}\} \tag{31}$$

and

$$\mathfrak{F}=\max\{0.0, F_{AD}(\Delta V)-V_{D,\text{gas}}\} \tag{32}$$

where AD is the acceptor or donor and ΔV the total volume flux which is positive by definition.

The first condition prevents more liquid than is available to be convected out of the donor cell (Fig. 3b), while the second condition prevents more gas than is available to be convected (Fig. 3c). Droplets are moved independently according to their own governing equations in the first step of the solution algorithm and are never convected along with the fluid in the third step. It should be remembered that as the function F moves with the fluid, its value is never changed except as a result of atomization or convection in the third step.

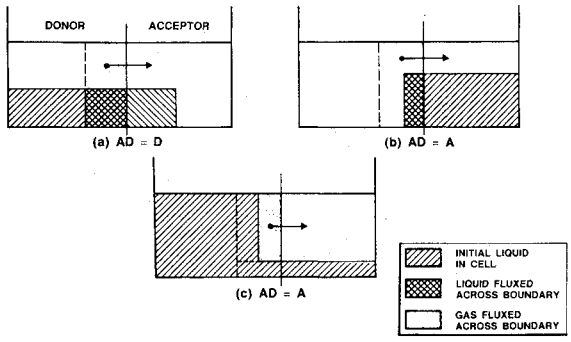

Fig. 3 Fluxing of cell volumes across cell boundaries (dashed line indicates boundary of total volume fluxed).

Semiempirical Physical Models

Thus far we have not defined the interphase interaction terms appearing in the governing equations for all three phases. Perhaps what distinguishes the task of combustion modeling from that of ordinary fluid-dynamics simulation is the large number of these interaction terms. Exact analytical expressions for these terms are unavailable because the physics governing these interaction processes are largely unknown; or even if they are, as in the case of turbulence-related phenomena, a direct numerical solution will be impractical. Thus, physical models based primarily on experimental correlation are employed. To complete the description of the present methodology, these models are discussed briefly below.

Droplet-Gas Interactions

The discrete droplets interact with the gaseous phase through the following exchanges: 1) momentum (droplet drag), 2) energy (droplet heatup), and 3) species (droplet evaporation). Currently, the expressions employed are the same as those in Ref. 14; namely,

$$m_k \frac{dH_k}{dt} = L(T_k)\frac{dm_k}{dt} + \underbrace{2\pi r_k K^*(T-T_k)[2+0.6(Re^{1/2}Pr^{1/3})^*]\left[\frac{(1-y_1^*)}{(1-y_1)}\right]}_{q_k} \tag{33}$$

for the droplet enthalpy change where $L(T_k)$ is the latent heat of vaporization. The vaporization rate is given by

$$\dot{m}_{evap} = \left(1-\frac{y_0}{y_0^*}\right)\left[\frac{Nu_m}{Nu_h}\right]\frac{q_K Le^*}{y_1(h_1-h_1^*)+y_0(h_0-h_0^*)} \tag{34}$$

where

$$Nu_m = 2+0.6(Re^*Sc^*)^{1/2} \tag{35}$$

and

$$Nu_h = 2+0.6(Re^*Pr^*)^{1/2} \tag{36}$$

Equations (33) and (34) are primarily valid for dilute subcritical drops. Eventually, they will be replaced with models more suitable for a dense, supercritical liquid-oxygen (LOX) spray environment, which is usually encountered in liquid rocket engines. The droplet drag coefficient per unit relative velocity, employed in Eq. (19), is assumed to be the sum of Stokes' drag and aerodynamic drag:

$$\mathfrak{D}_k = 6\pi\mu r_k + \tfrac{1}{2}\pi r_k^2 C_D |u_r| \tag{37}$$

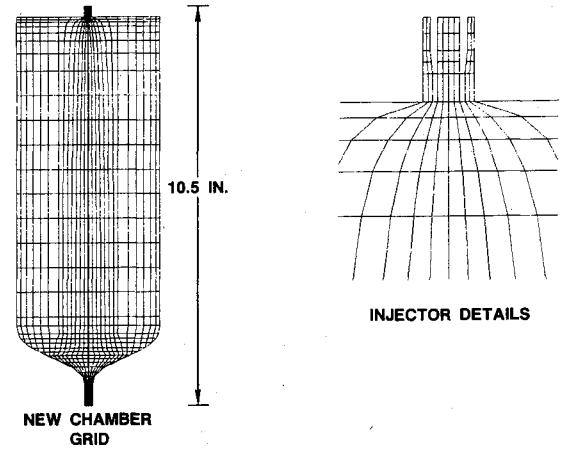

Fig. 4 Grid of injector/combustion chamber model.

where

$$|u_r| = [(u-U_k)^2+(v-V_k)^2+(w-W_k)^2]^{1/2}$$

Droplet-Liquid Interactions

The liquid and droplet phases interact through the process of atomization. The reverse process—a droplet reincorporating into the liquid if it hits the liquid surface—is also allowed. Atomization takes place only in cells where a free surface exists, but not in those that are fully gaseous or fully liquid. Currently, the empirical atomization model used is taken from Ref. 1 and involves the determination of a local mass stripping rate

$$\dot{M}_A = C_A\left[\frac{\mu_\ell(\rho u_r^2)^2}{\sigma_\ell/\rho_\ell}\right]^{1/3}\pi D_j(\Delta y) \tag{38}$$

and mean droplet diameter

$$\bar{d} = B_A\left[\frac{\mu_\ell(\sigma_\ell/\rho_\ell)^{1/2}}{\rho u_r^2}\right]^{2/3} \tag{39}$$

Equation (38) has the drawback that as the liquid jet diameter gets infinitesimally small, so does the atomization rate; possibly creating a very long, thin jet. From classical analysis,[16] it is known that a liquid jet becomes unstable and rapidly disintegrates when its free length is longer than its circumference. Based on this argument, D_j in Eq. (38) is replaced with ℓ_{jet}/π when such is the case, i.e.,

$$D_j = \max(D_j, \ell_{jet}/\pi) \tag{40}$$

The actual distribution of droplet sizes around the mean diameter, e.g., Gaussian or a flat distribution, is up to the user for the particular problem being treated. As these distribution functions are applied only *locally* for each cell, their choice makes little difference as long as there is a sufficient sampling rate. The empirical constants C_A and B_A need to be correlated from experimental data, which at present are still being determined for the case of LOX/H_2 under typical rocket chamber conditions. From initial experimentation with the model, however, it is found that their values should be on the order of

$$C_A = 0.0378 \quad \text{in the cup region}$$

$$= 0.14 \quad \text{in the main chamber}$$

$$B_A = 7836.4$$

Liquid-Gas Interaction

Currently no direct species exchange is allowed through evaporation or diffusion, as the amount involved is miniscule

compared to that between the gas and the droplets that have a much bigger surface area. Energy exchange is also neglected. Pressure differences due to surface tension can be calculated, although it is currently not in use for the simple coaxial liquid jet to avoid the additional computations necessary for determining surface curvatures. Since the gas and liquid phases are given uniform treatment within the same numerical framework, momentum exchange between the two phases is automatically taken care of. The only complication is to switch from the gaseous value for the laminar viscosity to that of the liquid when passing from one phase to the other. In cells where both phases are present, the lower gaseous value is adopted. Should better definition of the velocity profile and shear stresses within surface-containing cells be required, velocity rules similar to the law-of-the-wall functions used near solid surfaces can be employed.

Two more physical models concerning the gaseous phase only are also required to complete the picture.

Gas-Gas Chemistry

The oxygen-hydrogen chemistry has been investigated by various authors,[17] although no single set of equations has been proved to be suitable for all situations. The current model, taken also from Ref. 14, allows for both kinetic (slow reactions) and equilibrium (fast reactions) descriptions of the chemistry. It has been the experience of the first author of this paper that some rate-controlling reactions must be given in kinetic equation form for a proper prediction of transient phenomena such as flame-front propagation. On the other hand, in typical low mixture ratio (e.g., 1) hydrogen-oxygen streams, the flame often has difficulty sustaining itself in the absence of an ignition source if a strictly kinetic description is employed. The problem is physical as well as numerical, since a very tiny hot region acting as a flame holder is usually required to stabilize the flame, and finite grid resolution may not permit such a small localized hot zone to be modeled adequately. The problem is overcome if certain equilibrium equations are employed to signify instant reactions when the reactants are present. The current set of equilibrium and kinetic equations available in the model is listed in Table 2. Redundancy is present if all equations are used. For steady-state flame controlled by evaporation or atomization rates, use of the equilibrium equations only has given satisfactory results.

Turbulence Model

The eddy viscosity is modeled algebraically. The model[18] is intended to simulate mainly the time-dependent, larger-scale, freestream turbulence eddies. The total viscosity is written as a sum of three components:

$$\mu = \underset{\text{back-ground}}{\mu_0} + \underset{\text{lam-inar}}{\mu_{\text{lam}}} + \underset{\text{turbu-lent}}{\mu_t} \tag{41}$$

for which the turbulent viscosity is given by

$$\mu_t = 1/\sqrt{2}\rho\, K_D \Lambda^2 \|\underset{\approx}{\text{def}}\, \boldsymbol{u}\| \tag{42}$$

where $\|\underset{\approx}{\text{def}}\, \boldsymbol{u}\|$ is the magnitude of the velocity deformation tensor. Turbulent species diffusion and heat conduction are obtained from the turbulent viscosity assuming constant Schmidt and Prandtl numbers. Impact of combustion on the gas turbulence structure is not treated.

Drop-turbulence interactions are described using a random-walk model[13] based on a Gaussian distribution of local gas velocity perturbations. A turbulent kinetic energy level ϵ specified as a fraction of the mean flow kinetic energy, and a turbulence time scale τ are supplied by the user as constants backed out from experiments or as the results of turbulence models. The instantaneous gaseous velocity acting on the particle is then taken as

$$\boldsymbol{u} = \boldsymbol{u}_{\text{mean}} + \epsilon^{1/2} \text{sgn}(A,B) \text{erf}^{-1}(|A|, |B|) \tag{43}$$

where A,B are random variables uniformly selected from the range $(-1, +1)$. The velocity perturbation acts for a duration equal to τ. Anisotropic effects can be simulated by specifying a different ϵ for different directions if desired. This model is found to give realistic descriptions of the droplet dispersion phenomenon.

Table 2 H_2/O_2 reactions currently in use

Kinetic Reactions		
$H+O_2$	$\rightleftharpoons$	$O+OH$
H_2+O	$\rightleftharpoons$	$H+OH$
H_2O+O	$\rightleftharpoons$	$OH+OH$
H_2O+H	$\rightleftharpoons$	H_2+OH
H_2O_2+OH	$\rightleftharpoons$	H_2O+HO_2
HO_2+H	$\rightleftharpoons$	$2OH$
HO_2+H	$\rightleftharpoons$	H_2+O_2
$H_2O_2+O_2$	$\rightleftharpoons$	$2HO_2$
H_2O_2+H	$\rightleftharpoons$	HO_2+H_2
Equilibrium reactions		
O_2	$\rightleftharpoons$	$2O$
H_2	$\rightleftharpoons$	$2H$
H_2+O_2	$\rightleftharpoons$	$2OH$
$2H_2+O_2$	$\rightleftharpoons$	$2H_2O$

Examples

In the following, three examples are given to illustrate the qualitative features of the model.

Coaxial Injection Flame-Front Propagation

The grid model in Fig. 4 represents a test chamber for a coaxial gas-gas injector element. The chamber is prefilled with 1×10^6 dyne/cm^2 oxygen gas at 298 K. At the time zero hydrogen in the outer sleeve and oxygen in the center come in with an overall mixture ratio of 1. A "spark" ignition (energy) source is placed near the injector tip slightly off the centerline to initiate the combustion, and the final combusted mixture exits through the high contraction ratio nozzle into atmospheric pressure under choked conditions. Figure 5 summarizes the transient development of the expanding flame front, which is best defined by the presence of active OH radicals. As the original chamber oxygen is being used up, a smaller and more stable flame is established at the injector tip. The transient process lasts about 10 ms and would take about 50,000 s of CPU time on the CDC CYBER 176 to run through completion.

Liquid Injection and Atomization

In the second example, a concentric cryogenic LOX/H_2 stream replaces the gaseous streams of the previous example. The liquid oxygen has a density of 1.12 g/cm^3 and a temperature of 94.4 K. The gaseous hydrogen comes in at 6.895×10^6 dyne/cm^2 and atmospheric temperature, which are also the conditions for the hydrogen-prefilled chamber. The velocity differential between the two streams is high (8.47×10^3 cm/s for H_2 and 134 cm/s for LOX), resulting in a rapid atomization process specially in the recessed cup region Figure 6 shows the details of the evolution of the liquid jet. In Fig. 6a, the jet surface is not smooth because of the arbitrary way in which the jet shape is initialized at the beginning of the run. However, the effects of liquid-gas interaction and atomization eventually form the jet into a smooth pointed spike. No spark has been turned on and at these temperatures evaporization is minimal. The droplets shown thus correspond to an inert spray distribution. The spray cone distribution half-angle is approximately 25 deg.

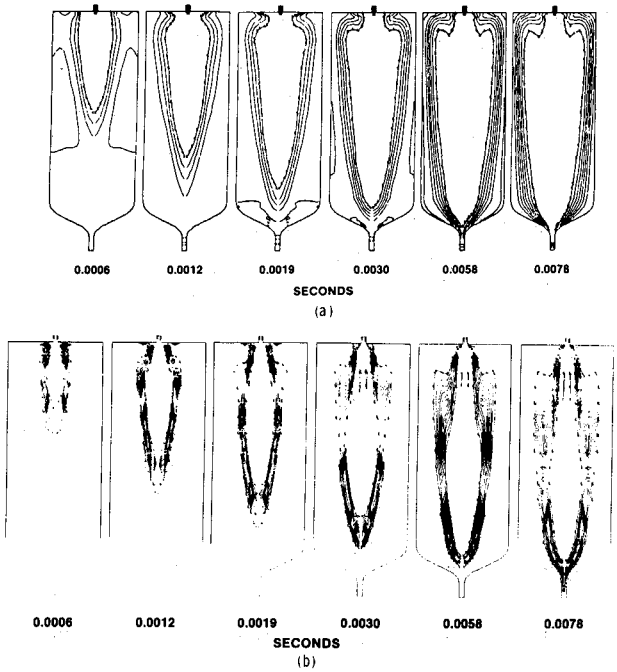

Fig. 5 Transient ignition in an O_2-prefilled chamber; a) density, b) OH mass fraction.

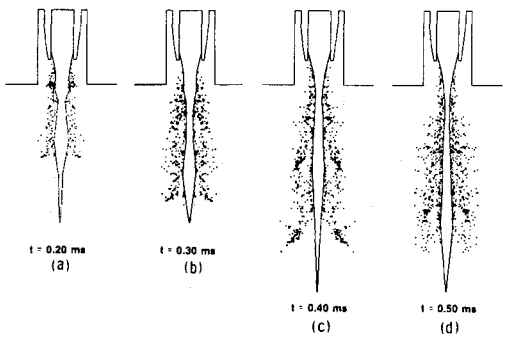

Fig. 6 Close-up details of an evolving liquid (LOX) jet.

Full Combustion Simulation

In this final example, the convergent nozzle chamber has been replaced with a straight tube section with "symmetry" (free-slip) walls. The study is conducted to simulate the conditions inside the SSME high-pressure fuel pump combustion chamber, which has 264 such identical elements injecting into one large cylindrical chamber. Injector i.d. is 0.226 cm and o.d. is 0.376 cm tapering at a 7-deg angle to 0.290 cm. Outer sleeve o.d. is 0.503 cm, and cup recess depth is 0.254 cm. The computational domain has a 1.628 cm diameter based on average area per unit element. Mass incoming flow rate, corresponding to a 109% power level operation of the SSME, is 158.3 g/s for LOX and 118.4 g/s for H_2. A small amount of hydrogen (25 g/s) also bleeds in uniformly through the entire faceplate. Inlet manifold pressure is around 4.15×10^8 dyne/cm^2 and overall chamber pressure is approximately 3.79×10^8 dyne $\times$ cm^2. Inflow temperatures for oxygen and hydrogen are 118 and 154 K, respectively.

The problem has been run through approximately 2 ms of physical time when the steady-state features of the combusting flow have become apparent. Figure 7 shows the representative velocity field, Fig. 8a is a typical jet-droplet distribution plot, and Fig. 8b the temperature field. The mixing of the hydrogen and the evaporated oxygen and the cooling effect of the bleed gas are all evident. The corresponding distributions of the

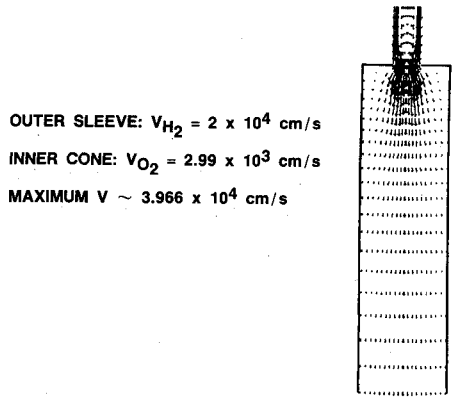

Fig. 7 Typical velocity field injecting into uniform tube (SSME, preburner coaxial element).

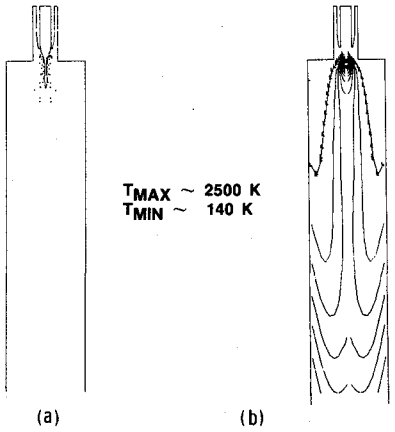

Fig. 8 SSME, preburner coaxial injector simulation; a) droplet spray and liquid-oxygen surface at $t = 0.119$ ms, b) isotherms.

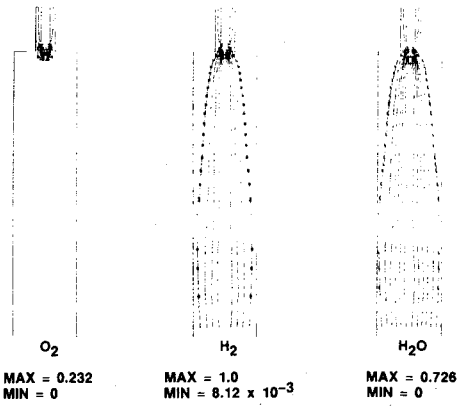

Fig. 9 Species mass fraction contour plots of oxygen, hydrogen, and water in simulated diffusion flame (SSME, preburner injector element).

three species, O_2, and H_2O, are shown in Fig. 9. Local peak temperature is in the 2000-K range, although average chamber temperature is closer to the adiabatic flame temperature of about 1500 K based on overall mixture ratio. The active reaction zone as revealed by the contour plots is enveloped by the cold bleed gas, and extends downstream to about 4 cm from the faceplate. As indicated in Fig. 8, few droplets survive in the combustion chamber, implying their relatively short lifespan (typically less than 0.1 ms for typical micron-size droplets). Thus, it appears that, atomization, not evaporation, may be the rate-controlling process. Detailed measurements of the experimental data will be required to confirm this hypothesis.

Summary and Conclusions

A viable tool has been developed that simulates all of the regions in a liquid-propellant combustion chamber flowfield in detail. With a fully coupled, three-phase capability and all of the interphase processes modeled, the degree of realism in the simulation potentially can surpass previously available capability. However, it is evident that while computer methodology has advanced, the increase in our experimental knowledge of these complex flows has not progressed quite nearly as fast as we would like. Yet such data are needed to define, refine, and verify the many empirical models still embodied in the simulation. The acuteness of the problem becomes more evident in the case of multiphase combusting flows. In particular, droplet size distribution data from atomization studies for the thick spray conditions is sorely lacking. For correct modeling of secondary atomization processes, the deformation and disintegration of droplets must be properly accounted for. These could well be the rate-controlling processes. On the other hand, the correct description of the chemical reactions for even O_2/H_2 combustion is far from being certain. The choice of describing a certain reaction as kinetic or equilibrium, combined with the effects of grid resolution, seems to have a marked effect on such issues as ignitability and flame steadiness. The role of the so-called third-body reactions is not well understood. The choice of the reaction set may well be problem- and grid-dependent; the latter being unavoidable because of the many different length scales involved.

However, it has been shown that a basic framework for simulation of thick spray flows is now available. In addition to being useful for actual hardware analysis, the tool also can be used to investigate and extend the range of validity of the physical models. Studies can be done both on a microscope scale, e.g., events surrounding a single deforming droplet, or on a global scale. Perhaps, this is where the model will prove most useful in the immediate future.

Acknowledgments

The authors would like to thank Dr. R. Jensen and Messrs. M. Varma and P. Reiser, Rocketdyne, and Drs. L. D. Cloutman, J. K. Dukowicz, J. D. Ramshaw, and A. A. Amsden, the authors of the CONCHAS-SPRAY code on which the current model is based, for their support. This work was carried out under NASA Contract NAS8-34928, monitored by Mr. D. Pryor of the Marshall Space Flight Center.

References

[1]Sutton, R.D., Schuman, M.D., and Chadwick, W.D., "Operating Manual for Injection Combustion Model," NASA-CR-129031, April 1974.

[2]Svehla, R.A. and McBride, B.J., "FORTRAN IV Computer Program for Calculation of Thermodynamic and Transport Properties of Complex Chemical Systems," NASA TND-7056, Jan. 1973.

[3]Schuman, M. D. and Beshore, D. G., "Standardized Distributed Energy Release 'SDER' Computer Program," AFRPL-TR-78-7, Aug. 1978.

[4]Schuman, M.D., Ervin, J., Taniguchi, M., Webber, W.T., and Wong, E.Y.C., "Transient Performance Programs," Vol. I, AFRPL-TR-80-22, Jan. 1981.

[5]Nickerson, G.R., Frey, H.M., and Coats, D.E., "Generalized Kinetic Analysis Program: A Computer Program for the Analysis of Chemically Reacting Gas Mixtures," Ultra Systems Inc. (formerly Dynamic Sciences), Irvine, CA, June 1971.

[6]Harsha, P.T. and Edelman, R.B., "Analytical Modeling of a Spray Diffusion Flame," AIAA Paper 84-1317, June 1984.

[7]Sturgess, G.J., Syed, S.A., and McManus, K.R., "Calculation of a Hollow-Cone Liquid Spray in a Uniform Air Stream," AIAA Paper 84-1322, June 1984.

[8]Liang, P.Y., "Liquid Rocket Combustor Computer Code Development," *Proceedings of the Advanced High-Pressure O_2/H_2 Technology Conference,* NASA CP-2372, June 1984, pp. 696-716.

[9]Liang, P.Y. and Chang, Y.M. "Development of Three Phase Combustion Code for Modeling Liquid Rocket Engines," Proceedings of the 21st JANNAF Combustion Meeting, Laurel, MD, Oct. 1984, Vol. 1, pp. 357-367.

[10]Nichols, B.D., Hirt, C.W., and Hotchkiss, R.S., "SOLA-VOF: A Solution Algorithm for Transient Flow with Multiple Free Boundaries," Los Alamos National Lab., Los Alamos, NM, Rep, LA-8355, Aug. 1980.

[11]Amsden, A.A., Ruppel, H.M., and Hirt, C.W., "SALE: A Simplified ALE Computer Program for Fluid Flow at All Flow Speeds," Los Alamos National Lab., Los Alamos, NM, Rept. LA-8095, June 1980.

[12]Amsden, A.A. and Ruppel, H.M., "SALE-3D: A Simplified ALE Computer Program for Calculating Three-Dimensional Fluid Flow," Los Alamos National Lab., Los Alamos, NM, Rept. LA-8905, Nov. 1981.

[13]Dukowicz, J.K., "A Particle-Fluid Numerical Model for Liquid Sprays," *Journal of Computational Physics,* Vol. 35, April 1980, pp. 229-253.

[14]Cloutman, L.C., Dukowicz, J.K., Ramshaw, J.D., and Amsden, A.A., "CONCHAS-SPRAY: A Computer Code for Reactive Flows with Fuel Sprays," Los Alamos National Lab., Los Alamos, NM, Rept. LA-9294-MS, May 1982.

[15]Hirt, C.W. and Nichols, B.D., "Adding Limited Compressibility to Incompressible Hydrocodes," *Journal of Computational Physics,* Vol. 34, No. 3, March, 1980, pp. 390-400.

[16]Giffen, E. and Muraszew, A., "The Mechanism of Disintegration of Liquid Jets," *The Atomization of Liquid Fuels,* 1st Ed., John Wiley & Sons, New York, 1953, Chap. 1, pp. 1-34.

[17]Westbrook, C.K., "Hydrogen Oxidation Kinetics in Detonations," *Journal of Combustion Science and Technology,* Vol. 29, No. 1, Jan. 1982, pp. 67-81.

[18]Deardorff, J. W., "On the Magnitude of the Subgrid Scale Eddy Coefficient," *Journal of Computational Physics,* Vol. 7, No. 1, Feb. 1971, pp. 120-133.